We greatly appreciate the thoughtful comments provided by the reviewers. We have given each considerable attention as described in the responses outlined below and have modified the manuscript in response to these comments.

Interactive comment on "Precipitation effects of giant cloud condensation nuclei artificially introduced into stratocumulus clouds" by E. Jung et al.

J. Jensen (Referee)
jbj@ucar.edu
Received and published: 6 March 2015

Major comments:
Interesting paper, likely effect demonstrated. That said there are some unresolved questions. If only one in 9 cases showed demonstrated effects of adding GCCN, then why did the other ones not. The authors suggest that it was due to clouds already precipitating. There may have been other reasons, e.g. insufficient cloud depth, etc.

We may have mislead the reviewers/readers by the statement "due to the ineffective seeding and sampling strategies on some flights and the presence of precipitation at the time of seeding on others, we are able to identify only one case on 3 August, 2011" in section 3.1. The primary reason that we did not see the effects of adding GCCN was due to the ineffective seeding and sampling strategies. For a given case, if the seeding and sampling strategies are definitely inadequate (such as no post-seeding sampling legs: 2-3 cases) we did not examine the case further. Accordingly, there were four less-than-ideal and two ideal cases of seeding experiments in terms of seeding and sampling strategy (Table1). Consequently we analyzed the two cases in detail in the same manner (3 August and 10 August 2011) and less detail for the four less-than-ideal seeding cases when the post-seeding cloud legs were located within the estimated seeding area. Based on these 7 cases (however, heavily relying on the two ideal cases, since the four less-than-ideal cases neither provided new insight nor altered the results shown for the two ideal cases) we concluded that the seeding effects were not effective when the cloud was already precipitating, since other conditions are relatively similar to each other or are closely related to precipitation production (such as cleaner environment in the presence of rain). It should be noted that the primary purpose of most of the flight plans (E-PEACE) was not the salt-seeding experiments.

To better understand the individual seeding cases, the summary of salt seeding experiments is given in Table 1 and the flight patterns of the individual 6 cases (two ideal, four less-than-ideal) are shown in Fig. 1, which are also shown in the Appendix A

in the modified manuscript. Further, a detailed analysis for 10 August case is shown in the last section of this response for a direct comparison with the 3 August 2011 case, which was shown in the manuscript. The text in the manuscript was modified to clarify that the flight patterns and sampling strategies for several of cases flown were inadequate for a complete analysis.

Table 1. Summary of salt seeding experiments

Date	Description	Cloud level (m) from Table 4 of Russell et al. (2015)
7/8	The TO did not sample the cloud after salt seeding. No post-seeding legs.	257-362 m (Thin cloud layer)
7/9	We performed two salt seeding experiments. However there was no post-seeding cloud-sampling leg for the first experiment. For the second experiment, the reference cloud legs (i.e., non-salted cloud sampling legs) were possibly contaminated by the first salt seeding experiment by the method shown in Fig. 5 in the manuscript.	283-570 m (Thick, wet cloud layer)
7/26	The seeding/sampling strategy was not an ideal (seeding and sampling pattern was perpendicular, and there was no sufficient post-seeding sampling). During the post-seeding flights in the mid-cloud and cloud-base heights, the seeded area was already advected far southeast. Only cloud top legs (post-seeding flight) were sampled from the estimated seeding area, and the seeding effects were shown at least in the cloud top leg.	253-560 m (Thick cloud layer)
7/29	NO post-seeding sampling legs. Right after injecting salt power, TO sampled the cloud at the same height as seeding, but it was found that the TO flew slightly above the seeding height (no LWC is detected).	265-534 m (High wet clouds)
8/2	The seeding/sampling strategy was not an ideal. Intersection with seeded area was small since the post-seeding was not made in the downstream of the seeding area. Seeding effect was not seen.	310-613 m (Thick, wet cloud layer)
8/3	Descent case solely based on the strategy (shown in the manuscript)	309-628 m (Thick cloud), *H~369 m
8/10	Descent case solely based on the strategy. However the cloud was already precipitating when it was seeded.	286-553 m (low clouds) *H~367m
8/11	The seeding/sampling strategy was not an ideal. During the mid-and cloud-top legs (post-seeding flight), the seeded area was already advected far southeast. Only cloud-base legs were (barely) located	440-600 m (Two broken cloud layers)

	within the seeded area.	
8/12	The seeding/sampling strategy was not an ideal. Post-seeding cloud sampling leg on the cloud-base only (barely) sampled the seeded area (no sufficient data for the post-seeding legs).	278-578 m (Thick cloud layer)

*H (cloud thickness) is calculated from the vertical profile of LWC obtained from soundings on the day (time and location is shown in Fig. 4 in the manuscript (for 3 August 2011) and in Fig. 5 shown later in this response (for 10 August 2011).

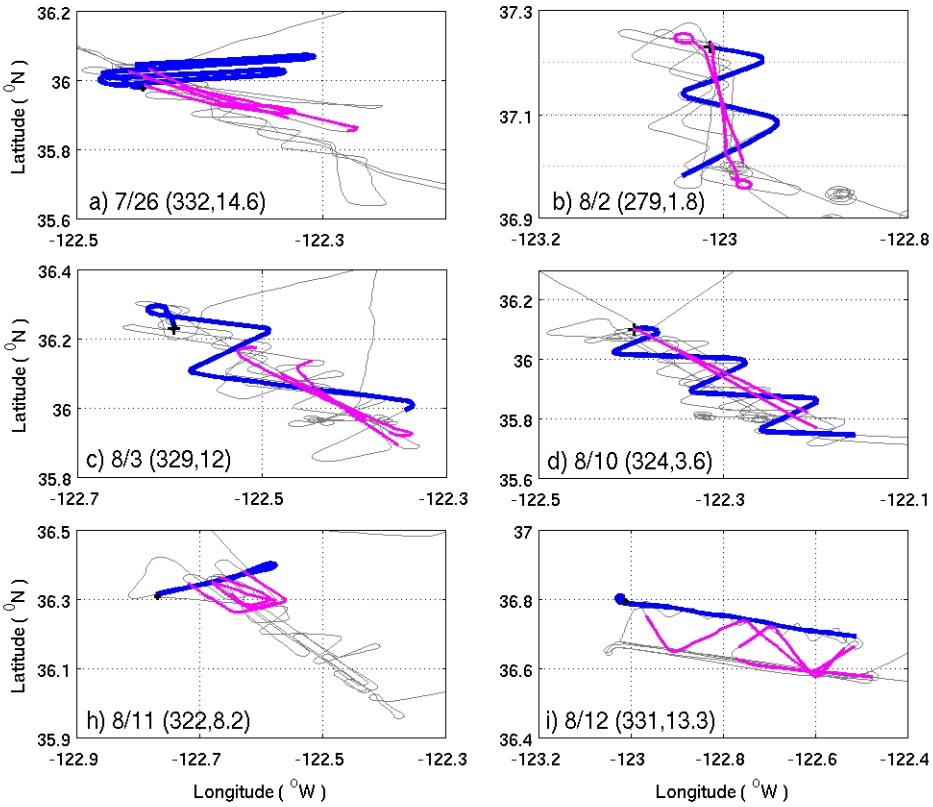

Fig. 1. Flight patterns during salt seeding (blue) and post-seeding cloud sampling legs (magenta) for some of the seeding flights. First and second numbers inside the parenthesis indicate the mean wind speed and wind direction during the salt-seeding leg.

In Fig. 1, the parallel post-seeding sampling with zigzag seeding pattern (c and d) was found to be the most effective flight pattern to capture the seeding effects. In contrast, the perpendicular patterns between the seeding and post-seeding patterns reduced the chance of proper sampling of a salted/seeded air mass during the post-seeding flights. In this case, there was no sufficient time for the seeded air mass to be sampled during the post-seeding sampling legs. Based on our analysis, the 3 August and 10 August cases were

ideal when the seeding and sampling strategy alone was considered. However, the cloud deck on 10 August was already precipitating while the seeding was made (confirmed with radar reflectivity, not shown).

1. The critical case with adding anthropogenic aerosols, in this case GCCN, is to know or estimate the natural amount of aerosols (GCCN). This is not done here. The authors estimate concentrations of their added GCCN, although this is at best done in a very approximate way.

To estimate the natural amount of aerosols (GCCN), aerosol concentrations larger than D > 2μm, D > 10 μm, D >20 μm were obtained from CAS on non-cloudy level flight legs flown near the ocean surface (20-30 m; 12 minutes of duration) and above the cloud top (750 m; 3 minutes of duration) as summarized in the table below.

Table 2. GCCN concentrations obtained from CAS on 3 August 2011.

	Near ocean surface (leg b in Fig. 4a in the manuscript)	~750 m (~ 17 UTC)
Diameter (μm)	Concentrations (cm^{-3})	Concentrations (cm^{-3})
D > 2	1.89	5×10^{-2}
D > 10	5.4×10^{-2}	3×10^{-3}
D > 20	9.5×10^{-3}	-

Table 2 shows that the natural amount of GCCN (e.g., D > 10 μm) above the cloud layer (~750 m) is on the order of 10^{-3} cm^{-3} and, no GCCN larger than 20 μm are observed there. On the other hand, the natural amount of GCCN with D > 10 μm near the ocean surface (about 20-30 m above the sea level) is on the order of 10^{-2}-10^{-3} cm^{-3}, which is an order of magnitude larger than those above the cloud layer. Table 1 also shows that the concentrations that are estimated for the salt dispersed artificially are at the same order as the GCCN concentration in nature. But we do not have an estimate just below cloud base to determine if this same concentration is available to the cloud. Also, there are uncertainties in these observed GCCN concentrations due to the low concentrations and the relatively small sampling volume of the CAS probe. Further, we acknowledge that our estimates of the emitted aerosols are crude too. These points have been added and clarified in the manuscript (page 10; lines 157-168 and Table 1 on page 29; highlighted as yellow colors).

2. There is no attempt at relating the injected concentrations of GCCN to drizzle drop concentrations larger that some critical size. Figure 7 shows an increase in the

concentration of drizzle drops, but with tick marks as sparse as 5 orders of magnitude, there is no real way of evaluating the concentration, let alone the increase in concentration, of drizzle drops. For instance, can the injected salt particles approximately explain the increase in drizzle drop concentrations, or are there so many more drizzle drops over such a large area that the injection of GCCN acted as a catalyst that initiated a subsequently much more efficient precipitation process in a cleaner environment?

To address this issue, we modified Figure 7 of the manuscript to include a y-axis with further resolution. In addition, we calculated total droplet number concentrations larger than different critical sizes (D > 50 μm, D > 100 μm, and D > 200 μm are used) to show the changes in drop number concentrations in these ranges before and after seeding and added these differences. The total droplet number concentrations for these calculations are obtained from CIP.

Table 3. Total droplets number concentrations larger than some critical sizes.

Diameter	**Total number concentration (cm^{-3}) obtained from CIP**		
D > 50 μm	**Before**	**After**	**Difference**
Cloud Top	0.81	1.26	0.45
mid-cloud	0.24	0.39	0.15
Cloud base	0.08	0.12	3.5×10^{-2}
D > 100 μm	**Before**	**After**	**Difference**
Cloud Top	2.7×10^{-2}	6.6×10^{-2}	3.9×10^{-2}
mid-cloud	1.2×10^{-2}	4.1×10^{-2}	2.9×10^{-2}
Cloud base	7.7×10^{-3}	3.4×10^{-2}	2.7×10^{-2}
D > 200 μm	**Before**	**After**	**Difference**
Cloud-top	3.3×10^{-4}	1.0×10^{-3}	7.1×10^{-4}
mid-cloud	2.9×10^{-4}	1.3×10^{-3}	1.6×10^{-4}
Cloud-base	3.1×10^{-4}	1.2×10^{-3}	1.6×10^{-4}

Table 3 shows the increase of GCCN number concentration by adding salt power. For instance, total number concentrations of GCCN larger than D > 50 μm increased by an order of 10^{-1} to 10^{-2} cm^{-3} in the cloud layer, and the largest increase is found at the cloud top height where the salt power is injected. The degree of increase in total number concentration decreases as the critical size increases, such as ~10^{-2} cm^{-3} increases for D > 100 μm and ~10^{-3} cm^{-3} to 10^{-4} cm^{-4} increase for D > 200 μm. These calculations show that the number of large droplets (e.g., D > 100 μm) does not exceed our crude estimates of the salt concentrations dispersed from the aircraft. We have included these changes in the large drop concentrations as Table 4 in the manuscript and have added a discussion of

this point to the text (pages 15-16; lines 273-284 and Table 4 on page 32; highlighted as yellow colors)

3. The authors attribute the change in cloud to seeding with GCCN, but were there other changes in the conditions experienced during the flight? For instance, did the near-surface wind speed change dramatically, thus explaining a natural increase or decrease in production of GCCN? Was the near-surface horizontal wind speed sufficient to explain wave breaking (10-m altitude speed above approx. 7 m/s)? Did the sea-surface temperature (SST) change in a way that might increase or decrease the turn-over time (residence time of cloud particles in cloud)? The manuscript does not address these causes of natural variability.

The mean wind near the ocean surface (~20 m) was about 10 m/s on this flight , so we cannot exclude the possibility of the contribution from the wave breaking (Please note that the aerosol number concentration (e.g., D > 10 μm) obtained from near the ocean level leg is an order higher than aerosol number concentrations obtained from above the cloud layer in Table 2). However, the winds remained almost the same before and after seeding experiment (Figure below) and the SST shows no variations either. We have modified the text to clarify these points (pages 10-11, lines 170-177 & page 17 lines 316-320; highlighted as yellow colors).

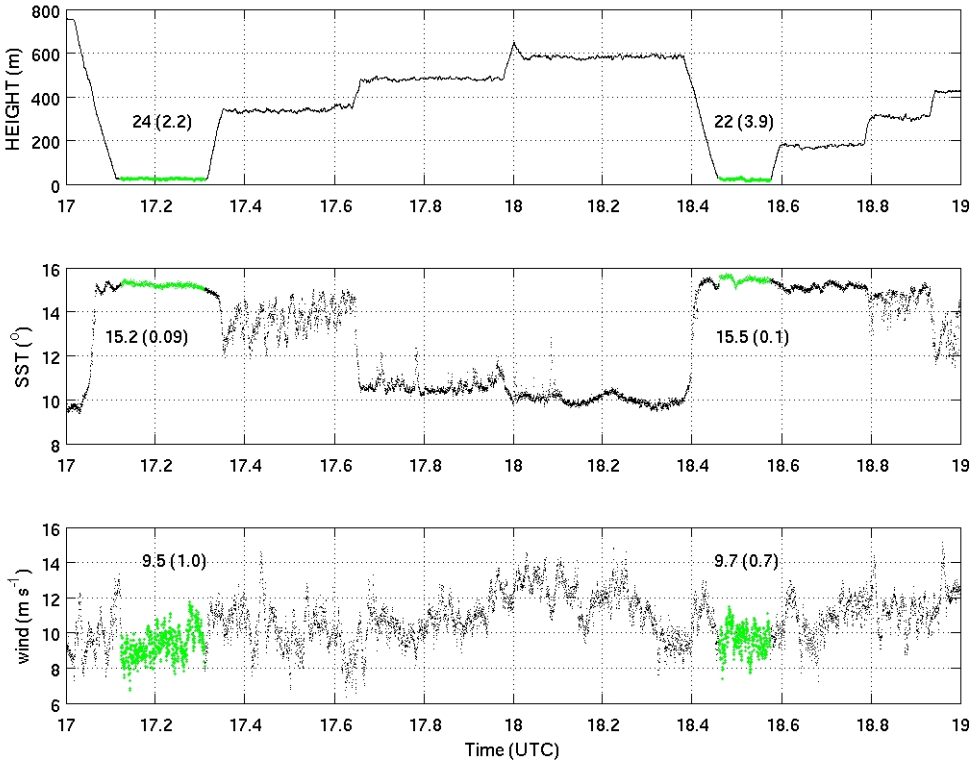

Fig. 3. Time-series of flight altitudes (upper), SST (middle), and wind speed (bottom)

during the flight on 3 August 2011. Data obtained from TO flying the closest the ocean surface before and after seeding is shown as green. Numbers indicate the mean (standard deviation).

Minor comments:

Page 57, line 13: "Typical time scale of 10-20 minutes." I think that is an underestimate, and anyway how was it determined? You have updraft and boundary-layer depths measurements to give much better estimates. My guess is that average updrafts were +0.4 m/s and average downdrafts were -0.4 m/s, which for a boundary-layer depth of 600 m would give t=2 x 600 / 0.4 = 3000 s or about 50 minutes.

We considered the cloud depth (H~300 m to 350 m) rather than the entire boundary layer depth since the salt power was injected at the cloud top, and updraft/downdraft ~ 0.5 m/s to 1 m/s; so t=2*300/0.5 ~ 20 minutes; t=2*350/1~10 minutes (~12 minutes for H=350 m, w=1 m/s; ~23 minutes for H=350, w=1 m/s.) We agree that the time underestimates the overturning time though the entire boundary layer. We recalculated the time by using cloud depth H~300-350m, vertical velocity w~0.35 (mean ranges from 0.3 to 0.4 (+0.2-0.3), and median values was about 0.3 m/s during the cloud layer). It gives t=2*350/0.35=33 minutes; t=2*300/0.35=29 minutes. We modified the manuscript accordingly from 10-20 minutes to 30 minutes and indicated that this is the overturning time within the cloud and may underestimate the overturning time through the depth of the boundary layer (page 14, line 247).

Page 58, line 7: "Appearance of a tail of large drops". Figure 7 does not show the generation of larger drops after seeding with GCCN; there is already a tail of large drops before seeding (all 3 boxes). However, the overall concentration of large drops certainly increases after the seeding.
Changes are made in the manuscript (page 15, line 267).

Page 73, figure 6 legend: If the CAS probe can measure drops in the size range 0-60 micron diameter, then average CAS observed diameters cannot exceed 60 micron, yet the plotted data show a significant number of mean diameters above 60 micron. I suspect that the mean is calculated from a combination of CAS and CIP data.
Changes are made in the manuscript (page 13, lines 220-224 and page 41 in Fig. 6).

Interactive comment on "Precipitation effects of giant cloud condensation nuclei artificially introduced into stratocumulus clouds" by E. Jung et al.

Anonymous Referee #2
Received and published: 24 January 2015

General Comments:
The effects of giant CCN on cloud and precipitation has been an important issue in weather modification and climate change, but is still poorly understood, due mostly to the lack of observational evidence. This article presents aircraft measurements of the changes in microphysical properties of stratocumulus clouds induced by seeding giant salt particles. The results are interesting and are well presented. It should be publishable in ACP if the following specific issues could be considered in revision.

Specific Comments:
1) During the "post-seeding" flights, did the aircraft fly over some clouds which are not influenced by the seeding? It would be more convincing if some evidence are provided to show that the drop size and number concentration in the seeded area are really different from those in the nearby areas which are not clearly influenced by seeding.

During the post-seeding flight, we tried our best to track the seeded area to examine the effect of adding salt. As a result, unfortunately we did not sample outside the cloud purposely. To answer this question at our best, we checked the flight on this particular day. There were three soundings after seeding (between 19:30 and 20:00 UTC in Fig. 4a in manuscript). However, one of them was sampled above the boundary layer (no cloud layer), and the other two soundings that include the cloud decks were sampled farther northeast close to coast (located outside the domain shown in Fig. 4), which is not comparable with current case of seeded air mass since the air mass closer to the coast is more polluted consisting of numerous smaller droplets. The reviewer's point motivates us to modify future plans for the salt seeding experiment to include the measurements of upstream along with downstream (seeded area) since we did not consider this earlier (Changes are not made in the manuscript)

2) The values shown in Table 2 should also include the standard deviations.
The standard deviations are given in the table (Table 3 on page 31).

3) In the caption of Figure 4, "Fig. 1f" should be "Fig. 4f"; the color "dark blue" is not really dark; other color curves are not clearly explained.

Changes are made in the manuscript (line 191 on page 11 and Fig. 4 on page 39).

Supplement to responses to Reviwer A---CASE OF 10 AUGUST 2011

(*please note that this part is not included in the modified manuscript)

Results form the case of 10 August 2011 are shown in Fig. 4 to Fig. 8. On 10 August 2011, the cloud depth are about 300-350 m, similar to that flown on 3 August, but the cloud base is lower on 10 August 2011. Accumulation mode aerosol concentration is about 200 cm^{-3} with little variability. The flight patterns (Fig. 5) are also similar to those flown on 3 August (Fig. 4 in the manuscript). Salt seeding is made during the cloud-top flights (shown as blue in Fig. 5f; 18:48-19:10 UTC), then the seeded area is sampled while the aircraft flies at cloud-base (g) and mid-cloud (h) heights from 19:30:37 to 19:53:23 UTC. On 10 August, no post-seeding cloud top legs are made. Figure 6 shows that the post-seeding cloud sampling area (red) is well located within the estimated post-seeding sampling area (shaded area), indicating that the seeded air-mass is properly sampled during the post-seeding legs. The size of cloud droplets for the day slightly increases after seeding (Fig. 7a), but the increase is insignificant compared with that observed on 3 August (Fig. 6a in the manuscript). Before seeding, cloud droplet number concentrations (Fig. 7b) are about 180-190 cm^{-3} through the cloud base to cloud top; they then decrease to 150-160 cm^{-3} after seeding. However, again, the decrease is not as significant as observed on 3 August. The mean precipitation rate (Fig. 7c) decreases after seeding, from 0.1-0.2 mm hr^{-1} to 0.1 mm hr^{-1}, though the median precipitation rate increases slightly from 0.04 mm hr^{-1} to 0.05-0.06 mm hr^{-1} (see Table 4).

Time series of radar reflectivity obtained from pre-seeding legs showed strong radar returns, confirming that the salt was injected to the cloud while it is precipitating (not shown). Changes in drop size distributions on 10 August, before and after seeding, are shown in Fig. 8. The different feature of DSD here, compared with that on 3 August 2011, is that there already are abundant large drops (e.g., D > 200 μm in Fig. 8a) prior to seeding at the level of cloud top where the salt seeding is made, which also reconfirm that seeding was made to the cloud that is already precipitating. After seeding, larger drops (in particular, D > 200 μm) are depleted significantly compared with those of pre-seeding condition in Fig. 8c. The rsults of 10 August is consistent with Feingold et al. (1999) in that seeding is not efficient for the precipitating cloud.

Table 4. As in Table 2 (in the manuscript), but for 10 August 2011. Median values of precipitation rate are denoted in the parenthesis.

8/10	D_e (μm)		N_d (cm^{-3})		R ($mm\ hr^{-1}$)	
	Before	After	Before	After	Before	After
Top	19.3 (21.3)	-	181	-	0.15 (0.05)	-
Mid	17.5 (19.3)	17.7 (19.3)	193	147	0.19 (0.04)	0.08 (0.06)
Base	14.8 (16.7)	14.6 (17.6)	185	159	0.12 (0.04)	0.07 (0.05)

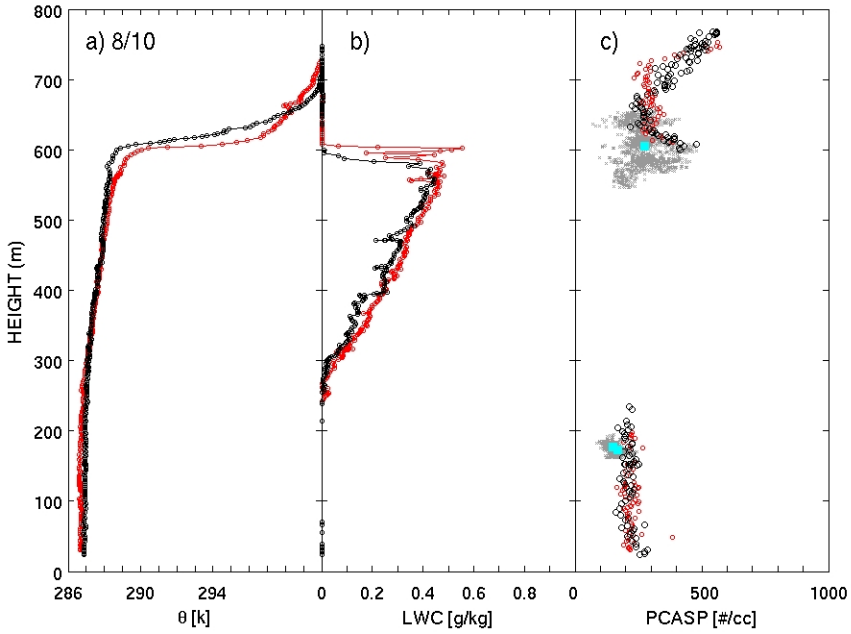

Fig. 4. As in Fig. 3 (in the manuscript), but for 10 August 2011.

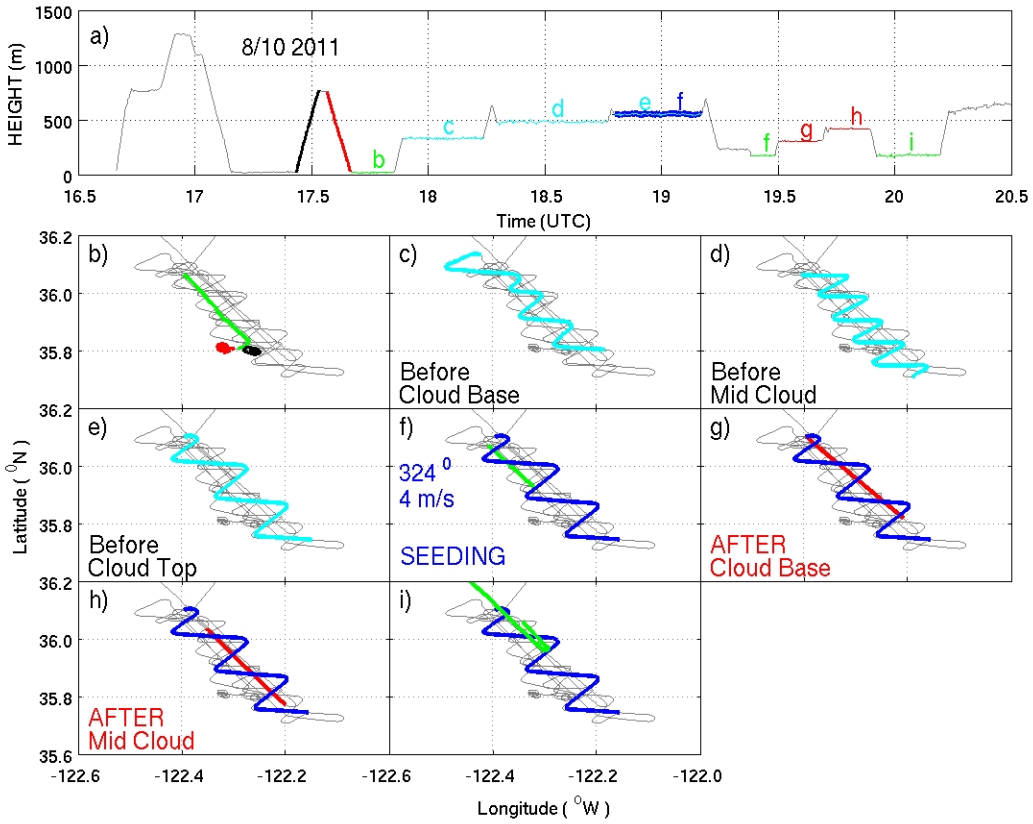

Fig. 5. As in Fig. 4 (in the manuscript), but for 10 August 2011.

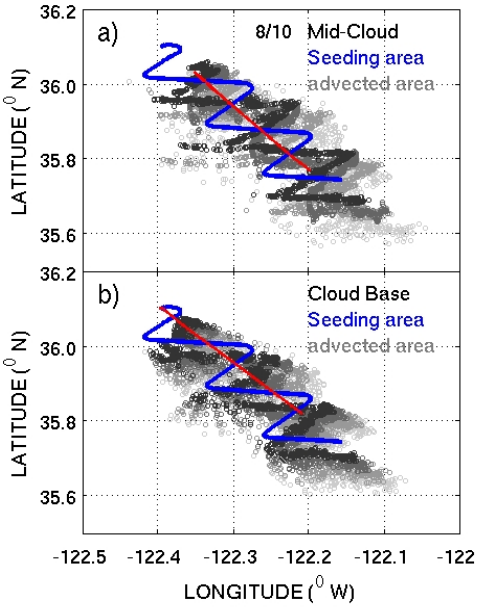

Fig. 6. As in Fig. 5, but for 10 August 2011.

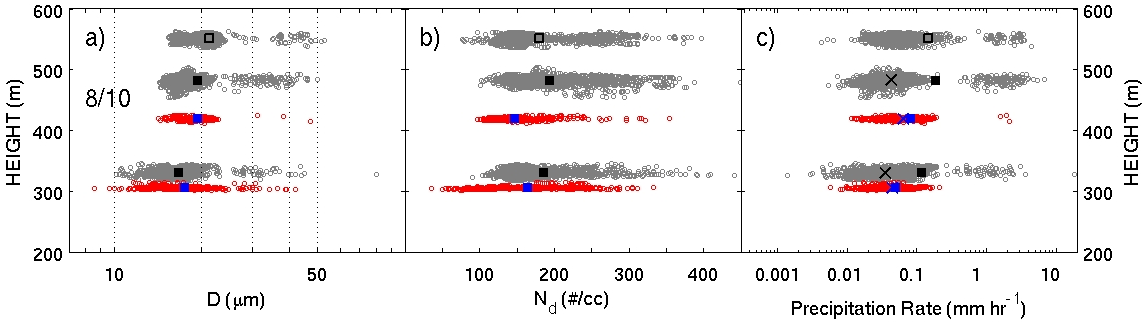

Fig. 7. As in Fig. 9 (in the manuscript).

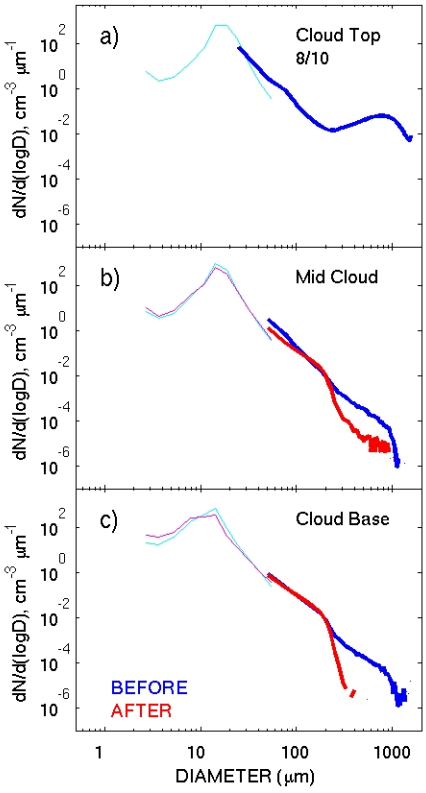

Fig. 8. As in Fig. 7 (in the manuscript), but for 10 August 2011.

Precipitation Effects of Giant Cloud Condensation Nuclei Artificially Introduced into Stratocumulus Clouds

Eunsil Jung[1], Bruce A. Albrecht[1], Haflidi H. Jonsson[2], Yi-Chun Chen[3,4], John H. Seinfeld[3],

Armin Sorooshian[5], Andrew R. Metcalf[3,6], Siwon Song[1], Ming Fang[1], Lynn M. Russell[7]

[1]Rosenstiel School of Marine and Atmospheric Science, University of Miami, Miami, FL, United States.

[2]Center for Interdisciplinary Remotely-Piloted Aircraft Studies, Naval Postgraduate School, Monterey, California, USA

[3]California Institute of Technology, Pasadena, California, USA

[4]Jet Propulsion Laboratory, California Institute of Technology, Pasadena, California, USA

[5]Department of Chemical and Environmental Engineering, and Department of Atmospheric Sciences, University of Arizona, Tucson, Arizona, USA

[6]Now at Department of Mechanical Engineering, University of Minnesota, Minneapolis, Minnesota, California, USA

[7]Scripps Institution of Oceanography, University of California, San Diego, La Jolla, California, USA

[1]Corresponding author address: Eunsil Jung, University of Miami, RSMAS/ATM,

4600 Rickenbacker Causeway, Miami, FL

Email: eunsil.jung@gmail.com

Abstract

To study the effect of giant cloud condensation nuclei (GCCN) on precipitation processes in stratocumulus clouds, 1-10 μm diameter salt particles (salt powder) were released from an aircraft while flying near cloud top on 3 August 2011 off the central coast of California. The seeded area was subsequently sampled from the aircraft that was equipped with aerosol, cloud, and precipitation probes and an upward-facing cloud radar. During post-seeding sampling, made 30-60 minutes after seeding, the mean cloud droplet size increased, the droplet number concentration decreased, and large drop (e.g., diameter larger than 10 μm) concentration increased. Average drizzle rates increased from about 0.05 mm hr^{-1} to 0.20 mm hr^{-1}, and liquid water path decreased from about 52 g m^{-2} to 43 g m^{-2}. Strong radar returns associated with drizzle were observed on the post-seeding cloud-base level-leg flights and were accompanied by a substantial depletion of the cloud liquid water content. The changes were large enough to suggest that the salt particles with concentrations estimated to be 10^{-2} to 10^{-4} cm^{-3} resulted in a four-fold increase in the cloud base rainfall rate and depletion of the cloud water due to rainout. In contrast, a case is shown where the cloud was already precipitating (on 10 August) and the effect of adding GCCN to the cloud was insignificant.

Keywords: E-PEACE, GCCN, Cloud Seeding, Precipitation, Stratocumulus Clouds

1 Introduction

The stratocumulus (Sc) cloud deck is the most persistent cloud type in the world, and the variations of the cloud amount and the albedo can significantly impact the climate system through their radiative effects on the earth system (e.g., Hartmann et al., 1992; Slingo, 1990). The addition of small amounts of giant cloud condensation nuclei (GCCN) to stratocumulus cloud may have little direct impact on radiative effects, but the impacts may be significant if the GCCN can initiate or enhance precipitation (Jensen and Lee, 2008). Nonetheless, the role of GCCN in precipitation production in stratocumulus clouds is less explored compared with the substantial work that has been done on other types of clouds (e.g., Takahashi, 1976; Johnson, 1982; Tzivion et al., 1994; Mather et al., 1997; Yin et al., 2000a,b; World Meteorological Organization, 2000; Levin et al., 2006; Rosenfeld et al., 2010). Therefore, our study focuses on the role of GCCN in stratocumulus clouds.

The role of GCCN in precipitation production in stratocumulus clouds has been explored using Large Eddy Simulation (LES) and parcel models (Feingold et al., 1999; Lu and Seinfeld, 2005; Jensen and Lee, 2008). These studies show that GCCN introduced into non-precipitating stratocumulus clouds can promote the growth of drizzle drops by enhancing collision and coalescence processes. Analysis of NASA A-Train data also suggest that enhanced levels of sea salt particles over the ocean lead to faster collision-coalescence and accelerated precipitation responses (L'Ecuyer et al., 2009; Sorooshian et al., 2013). Despite this basic understanding, observing the effects of GCCN in real clouds with in-situ measurements is challenging. First, GCCN concentrations in nature (order 10^{-4} to 10^{-2} cm^{-3}) are many orders of magnitude less than CCN concentrations (order 10^{2} cm^{-3}), and thus are difficult to measure. Second, cause-and-effect

relationships involving GCCN are difficult to isolate under natural conditions since other factors can affect and modulate drizzle production.

Marine stratocumulus clouds present laboratory-like conditions for evaluating how GCCN modify cloud properties. By introducing GCCN directly into a uniform cloud, the role that other factors may have in modifying the cloud can be minimized, and the background cloud conditions can be compared with the seeded cloud areas as shown by Ghate et al. (2007). The seeding by Ghate et al. (2007) used flares (in the size range of 0.1-2 μm) to produce hygroscopic particles in clouds ranging in size between 1 and 5 μm. The seeded cloud was then sampled with an instrumented aircraft flying within the Sc to examine the effects of the seeding on the cloud.

Flares, however, generate high number concentrations of small CCN particles simultaneous with much fewer giant CCN, and may not be optimal as seeder particles. Tzivion et al. (1994), Cooper et al. (1997), and Yin et al. (2000b), for example, showed that positive cloud responses to seeding (i.e., shift of size distribution toward larger sizes; enhanced precipitation) increase with the size of the seeding particles. In particular, the particles (diameter) smaller than 2 μm had a negative effect on the rain development in convective clouds (Yin et al., 2000b) based on the flares used in the South Africa seeding experiment (Mather et al., 1997). Furthermore, Segal et al. (2004), based on 2000-bin spectral cloud parcel model, predicted that hygroscopic-seeding materials with diameters of 3–6 μm are optimal for enhancing precipitation in warm clouds. They also predicted that smaller-sized CCN aerosols suppress precipitation as shown in Yin et al. (2000b) and L'Ecuyer et al. (2009). L'Ecuyer et al. (2009) showed that the injection of sea salt and sulfate aerosols into warm maritime clouds leads to nearly opposite cloud responses. The addition of large-sized sea salt particles was found to enhance precipitation and lead to less vertically developed clouds, whereas addition of the considerably smaller-sized

65 sulfate particles suppresses precipitation in clouds and results in the onset of light precipitation in
66 clouds with higher liquid water paths.

67 The purpose of this paper is to report on results from airborne flights examining the role
68 that GCCN play in initiating precipitation in Sc clouds. To introduce GCCN without increasing
69 the number of small-sized CCN that can suppress precipitation (e.g., Segal et al., 2007; L'Ecuyer
70 et al., 2009), we employed a technique developed by Rosenfeld et al. (2010) who injected milled
71 salt particles into convective cumuli. In the case we present here, GCCN in the form of milled
72 salt particles were dispersed into uniform Sc clouds from an aircraft flying near the cloud top.
73 After the GCCN were introduced into the cloud, the aircraft sampled the seeded cloud deck with
74 *in situ* instruments and an upward-facing cloud radar.

75

76 **2 Instruments and techniques**

77 **2.1 Aircraft data**

78 The data used in this study were obtained from the Center for Interdisciplinary Remotely Piloted
79 Aircraft Studies (CIRPAS) *Twin Otter* (TO) aircraft that was flown in support of the Eastern
80 Pacific Emitted Aerosol Cloud Experiment (E-PEACE, 2011), which took place off the central
81 coast of California during July and August 2011 (Russell et al., 2013). The CIRPAS TO research
82 aircraft was instrumented with (1) three *in-situ* probes that characterize aerosol, clouds, and
83 precipitation size distributions, (2) standard meteorological instruments that measure the
84 atmospheric thermodynamic and wind structures, and (3) an upward-facing Frequency
85 Modulated Continuous Wave (FMCW) cloud radar. Three probes relevant to this study were: (1)
86 Passive Cavity Aerosol Spectrometer Probe (PCASP), (2) Cloud Aerosol Spectrometer (CAS)
87 and, (3) Cloud Imaging Probe (CIP) that resolve particles in diameter ranges from 0.1–3 μm, 0.6-

60 μm and 25-1550 μm, respectively. The FMCW cloud radar (operating at a wavelength of 3 mm) was mounted on top of the aircraft, and provided fine structure of cloud and precipitation (vertical resolution of 5-m and temporal resolution of 3-Hz). The aerosol, cloud and precipitation probe data were obtained at 1-Hz resolution, and the meteorological variables (e.g., temperature, humidity, winds, Gerber probe liquid water content, etc) were acquired at both 1-Hz and 10-Hz resolutions. For detailed information on the probes and the cloud radar used in this study, see Russell et al. (2013), and Jung and Albrecht (2014, Table 1 and Fig. 1).

2.2 Salt Powder and Salt Distribution System

The salt powder comprises milled salt particles coated with an agent to minimize sticking as described by Rosenfeld et al. (2010). We measured the size distribution of the salt in the laboratory by delivering powder to the viewing volume of the CAS using an atomizer bottle. The number and volume (percent) size distribution are shown in Fig. 1. The number concentrations are relatively constant in the diameter range of 0.8 to 12 μm, with a peak in the volume distribution at 10-12 μm. There are relatively few particles smaller than 0.8 μm or larger than 12 μm. The effective volume diameter (i.e. the diameter that would give the average volume of the distribution) is about 5 μm.

To eject these particles from the aircraft into the clouds, we designed and fabricated a fluidized bed delivery system. The apparatus used an auger to feed salt powder at a controllable rate from a reservoir into a fluidized bed of sandblasting grit from which a filtered pump exhaust ejected the salt powder into the airstream outside the aircraft. The flow into the fluidized bed was

baffled to give a uniform airflow through a fine mesh membrane at the base of the bed, and the flow was adjusted such that the salt powder, but not the grit, was ejected. The purpose of delivering the powder through this fluidized bed was to break up salt particles that might be stuck together. Laboratory tests were carried out to determine auger delivery rates, and to determine proper flow rates to eject salt only while preserving the grit throughout the delivery. The salt delivery system was set to disperse the salt powder at a rate of about 0.75 g per second, which was intended to give GCCN concentrations of an order 10^{-2} to 10^{-4} cm^{-3}. For an average salt particle diameter of 5 μm, we estimate that about 5×10^{9} salt particles were emitted per second. A schematic and a photo of the salt powder delivery system are shown in Fig. 2.

Once the salt powder is emitted from the aircraft, it is dispersed, but the exact dispersal rate is unknown. The TO aircraft, with wing span of about 20 m, flew at a speed of about 60 m s^{-1} during the salt dispersal. Assuming that initial dispersion due to aircraft induced turbulence extends more than twice its wingspan, the salt plume cross-sectional area may be expected to quickly expand to about 50 m × 50 m. If 5×10^{9} particles are emitted along the 60 m path flown in 1 second, after 10 minutes, the salt concentration would then be about 3.5×10^{-2} cm^{-3}. If the cross sectional area of the plume expands to 100 m×100 m, the concentration would be reduced to about 1.7×10^{-2} cm^{-3}, and to about 1×10^{-3} cm^{-3} for a 200 m×200 m area. Thus, we estimate that after 10 minutes or more, the particle concentrations would be of the order of 10^{-2} to 10^{-3} cm^{-3}, which lies in the range used in simulations by Feingold et al. (1999).

3. Results

3.1 Seeding Case

During E-PEACE, salt powder was ejected into cloud decks during nine flights. However, due to the ineffective seeding and sampling strategies on some flights and the presence of precipitation at the time of seeding on others, we are able to identify only one case on 3 August, 2011 in which seeding impacts are evident throughout the entire cloud deck depth. But there are several cases showing seeding impacts exclusively at the cloud heights that are not precipitating at the time of seeding. It should be noted that the primary purpose of most of the flight plans (E-PEACE) was not the salt-seeding experiments. The summary of all the salt seeding experiments and flight patterns are shown in Fig. A1 and Table A1 in Appendix A to better understand the individual seeding cases. (These newly added parts are related to the reply to the reviewer (J. Jensen) for the overall major comments)

In this study we focus on the 3 August 2011 case when a Sc cloud deck was sampled with the TO in an area (35.8.1^{o} N-36.4.1^{o} N; 122.8^{o} W-122.2^{o} W) about 100 km southwest of Monterey between 16:00 UTC and 20:00 UTC. The boundary layer thermodynamic and aerosol vertical profiles, shown in Fig. 3, were obtained during a descent and an ascent of the aircraft through the cloud deck, approximately 10-30 minutes prior to flying horizontal background cloud-sampling legs, and about an hour prior to the cloud seeding (Fig. 4 and Table 1). The cloud deck was about 300-350 m thick (Fig. 3b) and capped by an inversion (with inversion strength $\Delta\theta$ of ~5-6K) at heights of about 625-645 m (Fig. 3). The inversion strength calculated from these two profiles is slightly weaker than those calculated from the entire period of the experiments ($\Delta\theta$ ~7$\pm$2K based on 25 flights). By comparison, these are weaker than those reported at the coast of northern Chile in the Southeastern Pacific during VOCALS-REx (e.g.,

~12K from Zheng et al., 2011). The cloud liquid water content (LWC) profiles, Fig. 3(b), are very consistent with those typical of a uniform, non-precipitating Sc cloud deck. The accumulation mode aerosol varies in concentration from 200 to 500 cm^{-3} in the sub-cloud layer in the ascent profile, and from 200 to 800 cm^{-3} above the cloud layer in both the ascent and the descent soundings (Fig. 3c).

To estimate the natural amount of GCCN, aerosol concentrations larger than D > 2μm, D > 10 μm, D >20 μm were obtained from CAS on non-cloudy level flight legs flown near the ocean surface (20-30 m; 12 minutes of duration) and above the cloud top (750 m; 3 minutes of duration) as summarized in Table 1. These estimates indicate that the natural amount of GCCN (e.g., D > 10 μm) above the cloud layer (~750 m) was on the order of 10^{-3} cm^{-3} and, no GCCN larger than 20 μm was observed there. On the other hand, the natural amount of aerosols of GCCN with D > 10 μm near the ocean surface (about 20-30 m above the sea level) was on the order of 10^{-2}-10^{-3} cm^{-3}, which was an order of magnitude larger than those above the cloud layer. Table 1 also showed that the GCCN concentrations in nature were at the same order as the GCCN concentrations that were estimated for the salt dispersed artificially. However, since no measurements of GCCN were made immediately below cloud base, we do not know the natural GCCN concentrations that were incorporated into the cloud. (These newly added parts are related to the reply to the reviewer (J. Jensen) for the major comments #1)

On this particular day, the mean wind near the ocean surface was about 10 m s^{-1} and thus, the higher concentration of GCCN near the ocean surface compared with those above the cloud layer was possibly contributed by the wave breaking. However, wind speeds near the ocean surface were nearly constant (9.5±0.8 ms^{-1}) during the flight. Further, since sea surface

174 temperature (SST) remained nearly constant during the flight (ranged from 15.2±0.09 °C to
175 15.5±0.1°C), no major changes in the surface buoyancy and moisture fluxes were experienced.
176 Therefore, there were no major changes in the background wind and the SST conditions that
177 could cause variability of GCCN during the sampling legs of this flight. (These newly added
178 parts are related to the reply to the reviewer (J. Jensen) for the major comments #3)

179

180 **3.2 Sampling Strategy**

181 Flight paths and time series of the altitudes flown on 3 August 2011 are shown in Fig. 4.
182 Detailed information of each leg segment is summarized in Table 2. To characterize the
183 background conditions, the clouds and the aerosol beneath them were sampled with *in situ*
184 probes and the cloud radar at four altitude levels, including one sub-cloud layer and three cloud
185 levels before the seeding (Figs. 4b, 4c, 4d, 4e), hereafter referred to as *pre-seeding (cloud*
186 *sampling) legs*. The seeding flight pattern is shown in Fig. 4f. After seeding, the seeded cloud
187 was sampled downwind of the seeded area at similar levels as characterized before (hereafter
188 referred to as *post-seeding (cloud sampling) legs*). To ensure that the seeded areas were sampled,
189 the post-seeding sampling areas (red in Figures. 4g, 4h, 4i) were selected by using wind speed
190 and wind direction measurements along the seeding path to advect the seed plume downstream.

191 The salt powder was dispersed as the TO flew near the cloud top (shown as thick blue in
192 Fig. 4f-j). Note that this seeding flight pattern is almost identical to the pre-seeding cloud top leg
193 (Fig. 4e). During the seeding, the wind was 12 m s^{-1} from the northwest (~330 °). After seeding,
194 the seeded air mass was sampled along the wind near cloud base (Fig. 4g), mid-cloud (Fig. 4h),

and near cloud top (Fig. 4i). These post-seeding legs were made about 30-60 minutes after the clouds were seeded (Fig. 4a and Table 2).

The estimated post-seeding areas at cloud top, mid-cloud and cloud-base are shown in Fig. 5 (gray shades), along with the seeding and post-seeding leg patterns. Here, the seeding pattern has been advected using the winds and elapsed time between seeding and post-seeding cloud sampling periods. If the cloud is seeded between A (starting time of seeding legs) and A′ (ending-time of seeding legs), and the post-seeding legs are made between B (starting-time of post-seeding legs) and B′ (ending-time of post-seeding legs), then four elapsed time periods are possible; (1) A′-B, (2) A′-B′, (3) A-B, and (4) A-B′. Here, A′-B (A-B′) corresponds to the shortest (longest) elapsed time periods between the time of seeding and post-seeding and shown as the darkest (lightest) colors in Fig. 5. The post-seeding sampling-pattern (red) is located well within the advected (shaded) areas, showing that the seeded area is properly sampled during the post-seeding cloud sampling leg. To compare changes in cloud and precipitation properties between pre- and post-seeding legs, post-seeding data from cloud sampling legs (red) made within the advected seeding area (i.e., gray shades) are used.

3.3 Seeding Results

Cloud droplet size (effective diameter, D), number concentrations (N_d), and precipitation rate (R) measured on the pre- and post-seeding legs are shown in Fig. 6. The number concentration of cloud droplets is obtained from the Cloud Aerosol Spectrometer (CAS). The precipitation rate is calculated from the Cloud Imaging Probe (CIP) drop size distributions *N(D)* as

$R = \frac{\pi}{6}\int_0^\infty N(D)D^3u(D)dD$, where *u(D)* is the fall speed of particle size *D* (Rogers and Yau, 1989*)*. The effective diameter is calculated in two ways: (i) first, it is calculated from drop size distributions (DSDs) obtained from CAS to show the changes in cloud droplet size exclusively (shown as numbers in Table 2); (ii) second, it is calculated from DSDs obtained by combining the CAS and CIP probes data to include cloud droplets, drizzle and rain drop embryos (shown in Fig. 6a as well as shown as numbers in parenthesis in Table 3). The first two channels (or bins) from the CIP probe overlap with the last two bins of the CAS, but the CIP has poor accuracy relative to the CAS for the overlapped ranges, so that the first two CIP size-bins were discarded when the data is combined.

Before seeding (grey in Fig. 6a), the majority of droplets had diameters between 10 μm and 30 μm. After seeding, the main population showed a significant broadening and an increase in sizes from a few μm to hundreds of μm. The mean effective diameter of cloud droplets was between 13.5 μm and 21.4 μm from the pre-seeding legs, and between 16.6 μm and 26.2 μm from the post-seeding legs (Table 3). The mean effective diameter of droplets that include drizzle and rain drop embryos (*D* shown in the parenthesis in Table 3) ranged between ~15 μm and 23 μm for the pre-seeding legs, and between ~24 μm and 44 μm for the post-seeding legs, suggestive of an increase in size of drizzle and rain drop embryos more than that of cloud droplets after seeding. Further, a substantial decrease in cloud droplet number concentration (N_d) was also observed during post-seeding legs (Fig. 6b, Table 3). The mean N_d calculated from pre-seeding legs was about 140-170 cm^{-3} throughout the cloud, and was reduced to about 70-100 cm^{-3} after seeding, which is consistent with what would be expected with enhanced droplet collision-coalescence. Precipitation rates (Fig. 6c, Table 3) were less than 0.1 mm hr^{-1} (0.04-0.09 mm hr^{-1})

238 before seeding and increased to about 0.2 mm hr^{-1} after seeding. The LWC, before and after
239 seeding, are also summarized in Table 3. After seeding, LWC decreased to about 0.04-0.25 g m^{-3}
240 from 0.09-0.31 g m^{-3}. Liquid water path (LWP) was calculated by integrating an average LWC at
241 cloud-base, mid-cloud, and cloud-top levels during pre- and post-seeding cloud sampling, after
242 they were linearly interpolated with height. The LWP was about 52 g m^{-2} before seeding, and
243 decreased to about 43 g m^{-2} after seeding.

244 As noted above, the post-seeding legs were made about 30 minutes to 1-hour after the
245 cloud was seeded (Table 2), allowing sufficient time for the salt seeding effects to be distributed
246 throughout the cloud due to large eddy transport through the depth of the boundary layer
247 operating on characteristic time scales of about 30 minutes. In the flare seeding by Ghate et al.
248 (2007), the post-seeding sampling was made about 10 to 30 minutes after the flare burns. In that
249 case, the effects on the droplet size distribution are clearly seen, but no drizzle was observed.
250 The lack of observable drizzle in those experiments may have been partly due to the premature
251 post-seeding cloud sampling (i.e., 10 to 30 minutes after seeding), but may also have been due to
252 the nature of the flares that they used, which produce higher concentration of smaller-sized salt
253 particles than the salt power used in this experiment.

254 Changes in drop size distributions, before and after seeding, are shown in Fig. 7. Overall,
255 number concentration of smaller sized cloud droplets (e.g., D < 20-50 μm) decreased during the
256 post-seeding legs (see the changes between blue and red), whereas the number concentration of
257 large droplets (D > 50 μm) increased. The decrease in smaller sized droplets concentration is
258 large at the cloud top where the GCCN is directly injected, and also near the cloud base. The
259 maximum diameter, at which the depletion of small-sized-droplets occurred, increased closer to

the cloud base. For example, near cloud tops, droplets smaller than 20 μm decreased in number substantially. At cloud base, number concentrations of droplets smaller than 50 μm have decreased. The increase in larger-sized-droplets during the post-seeding legs was substantial through all three-cloud level-legs. In particular, bimodal patterns were observed at the cloud base in the ranges between 50 μm and ~200 μm, and between 300 μm and ~1000 μm. Increases in larger drops (e.g., D > 50 μm) and decreases in smaller-sized-droplets (e.g., D < 20 - 30 μm) during post-seeding legs are consistent with the enhancement of collision-coalescence effects due to the salt. These changes in the droplet distributions in the seeded areas (i.e., enhancement of a tail of large drops on the upper end of droplet distribution) are similar to those reported by Ghate et al. (2007) in areas of Sc clouds seeded by flares, and by Rosenfeld et al. (2002) in the convective clouds seeded by GCCN, as well as by other numerical experiments on the impact of GCCN on precipitation and cloud structures (e.g., Johnson, 1982; Cooper et al., 1997; Rosenfeld et al., 2010).

In an attempt to relate the injected concentrations of GCCN to drizzle drop concentrations, changes in droplet number concentrations for drops larger than 50 μm, 100 μm, and 200 μm are calculated for the periods of pre- and post-seeding legs (Table 4). Drizzle drop number concentrations are calculated from CIP probe, and the numbers are average concentrations at three cloud levels (cloud-top, mid-cloud, cloud-base). In table 4, the total number concentrations of GCCN larger than D > 50 μm increased by an order of 10^{-1} cm^{-3} to 10^{-2} cm^{-3} in the cloud layer. Further, the greatest increase was found at the cloud top height where the salt power was injected for all-three critical sizes (not shown). The degree of increase in total number concentration decreased as the critical size increased, such as an increase of GCCN

concentration of about 10^{-2} cm^{-3} for D > 100 μm, and about 10^{-3} to 10^{-4} cm^{-3} for D > 200 μm. These calculations showed that the increase in concentrations of larger droplets was the same order of magnitude as our estimates of the salt concentrations dispersed from the aircraft. (These newly added parts are related to the reply to the reviewer (J. Jensen) for the major comments #2)

Radar returns from the upward facing cloud radar during the cloud-base level legs, before and after seeding, are shown in Fig. 8. Cloud-base level legs were conducted with the TO flying near the cloud-base altitude at average height of 339 m and 307 m during the pre- and post-seeding legs, respectively. Before seeding, (Fig. 8a), radar returns reached about 270 m above the level leg altitude (i.e., 609 m mean sea level (MSL); 270 m above radar level + 339 m from the ground), and the radar reflectivity was on average about -37 dBz with maximum of -25 dBz in a height range of 50 m and 100 m above the radar, for example. During the post-seeding legs (Fig. 8b), radar echoes appeared up to about 300 m above the level leg altitude (i.e., ~ 607 m MSL). The average radar reflectivity between 18:49:32 and 18:49:40 in a height range of 50 m and 100 m, for example, was about -21 dBz with maximum of -18 dBz. The radar measurements in Fig. 8 showed a significant increase in radar returns during the post-seeding legs compared with the pre-seeding legs, although the cloud-top height and cloud depths are nearly identical for the two cases.

The time series of radar reflectivity for the period of increased radar reflectivity (box in Fig. 8b) was shown in Fig. 8c along with LWC and drizzle rates (Fig. 8d). In Fig. 8d, LWC decreased as drizzle rates increased, indicating that drizzle may be consuming the cloud water. In Fig. 8(c-d), the variability in the radar reflectivity was clearly correlated with the drizzle rates observed at this level and inversely correlated with the cloud liquid water content.

We further calculated the radar reflectivity at the level of cloud legs by combining data from the cloud and precipitation probes before and after seeding as comparison to the actual radar measurements. Radar reflectivity is calculated as $z = \int N(D)D^6 dD$ where $N(D)$ is the drop size distribution (DSD) of particle size D, which is obtained from CAS and CIP, in units of mm^6m^{-3}. Radar reflectivity Z is reported in units of dBz, where Z=10log(z). The calculated median radar reflectivities for pre- and post-seeding legs were -32 dBz < Z < -31dBz, and -17 dBz < Z < -14 dBz, respectively (Table 2), which is consistent with typical values of Z for non-precipitating and precipitating clouds (Jung 2012; Frisch et al., 1995). The large changes in the radar reflectivity between the pre- and post-seeding cloud-base legs (Fig. 8) were consistent with the changes in the calculated reflectivity (Table 3).

Clouds were seeded on another TO flight made on 10 August (details not shown here). Although a similar effective seeding and sampling strategy was used on that flight (Fig. A1), no additional precipitation enhancement was noted. The cloud depth on the day was about 300-350 m, similar to that on 3 August (Table A1) but with lower cloud bases. The cloud deck was precipitating at the time of seeding (confirmed with radar reflectivity and drop size distribution, not shown), and the accumulation mode aerosol was less than 200 cm^{-3} in the boundary layer with little variation (not shown). (These changes are also related to the reply to the reviewer (J. Jensen) for the major comments #3)

Changes in cloud droplet size (D), number concentrations (N_d), and precipitation rate (R) between the pre- and post-seeding legs are shown in Fig. 9 for the 10 August case. Before seeding, cloud droplet number concentrations were about 180-190 cm^{-3} from cloud base to cloud top; they then decreased to 150-160 cm^{-3} after seeding. However, the decrease is not as large as

326 that observed on 3 August. The mean precipitation rate (Fig. 9c) decreased after seeding, from
327 0.15 mm hr^{-1} to 0.1 mm hr^{-1}, though the median precipitation rate was almost the same and/or
328 slightly enhanced from 0.04 mm hr^{-1} to 0.05-0.06 mm hr^{-1}. These results are consistent with the
329 previous modeling results, which demonstrate that the injection of GCCN has the greatest
330 potential for altering cloud behavior in non-precipitating clouds having a high concentration of
331 small drops and/or aerosol (e.g., Feingold et al., 1999; Yin et al. (2000a); Lu and Seinfeld, 2005;
332 Zhang et al., 2006; Jensen and Lee, 2008), and hence, conditions on 10 August 2011 were not
333 optimal for generating a strong precipitation signal, as confirmed by our measurements.

334

335 **4 Summary and Conclusions**

336 To study the effect of giant cloud condensation nuclei (GCCN) on precipitation in Sc clouds, we
337 released 1-10 μm diameter salt particles from an aircraft while flying near cloud tops during the
338 Eastern Pacific Emitted Aerosol Cloud Experiment (E-PEACE, 2011). Results from the 3 August
339 2011 flight provide evidence for a strong change in droplet number and size in the clouds that
340 were seeded with giant nuclei. The GCCN were released in a cross-wind zigzag pattern at a fixed
341 level (near cloud top) in a uniform cloud deck using a device designed to minimize the clumping
342 of the salt and provide concentrations in the range of 10^{-2} to 10^{-4} cm^{-3}. The seeded area was then
343 sampled downstream as estimated by advection of the area using observed winds and the elapsed
344 time between seeding and post-seeding cloud sampling periods. During the post-seeding cloud
345 sampling legs, conducted 30-60 minutes after seeding, the mean cloud droplet size had increased,
346 droplet number concentrations decreased and large drops appeared in the size distributions.
347 Average drizzle rates increased from about 0.05 mm hr^{-1} to 0.20 mm hr^{-1}. Strong radar returns

348 associated with drizzle were observed on the post-seeding cloud-base legs and were
349 accompanied by a substantial depletion of the cloud liquid water content. The changes were large
350 enough to suggest that the salt seeding resulted in a four-fold increase in the cloud base rainfall
351 rate and an associated depletion of the cloud water due to rainout. The reduction of cloud droplet
352 number concentrations indicates invigorated collision-coalescence between drops. Furthermore,
353 the drop diameter at all altitudes in the cloud deck increased in the seeded area. Thus, the
354 observational evidence confirms the particular chain of events that is expected after a cloud
355 seeding event: faster onset of rain owing to the broadening of cloud drop distribution.

356 The results show the enhancement of precipitation by artificially introducing GCCN into
357 a stratocumulus cloud. As in Ghate et al. (2007), the usefulness of marine Sc clouds to study
358 cause-and-effect relationships associated with GCCN is demonstrated. However, tracking the
359 exact movement of the cloudy air mass that has been seeded with GCCN using a single aircraft is
360 challenging. Use of tracers such as radar chaff (Jung and Albrecht, 2014) or SF_6 (Rosenfeld et al.,
361 2002; 2010) for tracking the seeded areas would facilitate these studies of cloud modification by
362 GCCN. Furthermore, a scanning-cloud-radar would provide a full view of the 3D temporal
363 evolution of the cloud in which GCCN are injected. Nevertheless, the results in this study
364 support the idea that giant nuclei—produced either naturally or anthropogenically—can initiate
365 drizzle and impact the cloud structure as shown in Levin et al. (2005) for dust aerosols coated
366 with sea salt and sulfate during the Mediterranean Israeli Dust Experiment campaign. Since the
367 concentrations of GCCN used in this study are in the range of those observed in nature under
368 strong wind conditions, we concur with the conclusions of Jensen and Lee (2008) that it may be
369 necessary to include GCCN effects in climate models.

370

5 Acknowledgements

The E-PEACE field campaign and modeling studies were funded by the National Science Foundation (AGS-1013423; AGS-1008848; AGS-1013381; AGS-1013319; ATM-0744636; AGS-0821599; ATM- 0349015) and the Office of Naval Research (N00014-11-1-0783; N00014-10-1-0811; N00014-10-1-0200; N00014-08-1-0465). The authors gratefully acknowledge the crew of the CIRPAS Twin Otter for their assistances during the field campaign and Dr. Daniel Rosenfeld for providing the powdered salt. We also appreciate the outstanding efforts of Tom Snowdon on the design and fabrication of the salt-powder dispensing system. We greatly appreciate the thoughtful comments provided by the reviewer Dr. Jorgen Jensen.

References

Cooper, W. A., Bruintjes, R. T. and Mather, G. K.: Calculations pertaining to hygroscopic seeding with flares, J. Appl. Meteorol., 36, 1449–1469, doi: http://dx.doi.org/10.1175/1520-0450(1997)036<1449:CPTHSW>2.0.CO;2, 1997.

Feingold, G., Cotton, W. R., Kreidenweis, S. M., and Davis, J. T.: The impact of giant cloud condensation nuclei on drizzle formation in stratocumulus: Implications for cloud radiative properties. J Atmos Sci., 56, 4100-4117, 1999.

Frisch, A. S., Fairall, C. W. and Snider, J. B.: Measurement of stratus cloud and drizzle parameters in ASTEX with a K α -Band Doppler Radar and a microwave radiometer, J. Atmos. Sci., 52, 2788–2799, doi: http://dx.doi.org/10.1175/1520-0469(1995)052<2788:MOSCAD>2.0.CO;2, 1995.

Ghate, V. P., Albrecht, B. a., Kollias, P., Jonsson, H. H. and Breed, D. W.: Cloud seeding as a technique for studying aerosol-cloud interactions in marine stratocumulus, Geophys. Res. Lett., 34(14), L14807, doi:10.1029/2007GL029748, 2007.

Hartmann, D. L., Ockert-Bell, M. E., and Michelsen, M. L.: The effect of cloud type on earth's energy balance - Global analysis. J. Climate, 5, 1281–1304, 1992.

Jensen, J. B. and Lee, S.: Giant sea-salt aerosols and warm rain formation in marine stratocumulus, J. Atmos. Sci., 65(12), 3678–3694, doi:10.1175/2008JAS2617.1, 2008.

399 Johnson, D.: The role of giant and ultragiant aerosol particles in warm rain initiation, J.
400 Atmos. Sci., 39, 448-460, 1982.

401 Jung, E.: Aerosol-cloud-precipitation interactions in the trade wind boundary layer, [online]
402 Available from: http://gradworks.umi.com/35/49/3549376.html (Accessed 6 November
403 2014), 2012.

404 Jung, E. and Albrecht, B.: Use of radar chaff for studying circulations in and around shallow
405 cumulus clouds, J. Appl. Meteorol. Climatol., 53(8), 2058–2071, doi:10.1175/JAMC-D-
406 13-0255.1, 2014.

407 L'Ecuyer, T. S., Berg, W., Haynes, J., Lebsock, M. and Takemura, T.: Global observations of
408 aerosol impacts on precipitation occurrence in warm maritime clouds, J. Geophys. Res.
409 Atmos., 114, D09211, doi:10.1029/2008JD011273, 2009.

410 Levin, Z.: On the interactions of mineral dust, sea-salt particles, and clouds: A measurement
411 and modeling study from the Mediterranean Israeli Dust Experiment campaign, J.
412 Geophys. Res., 110(D20), D20202, doi:10.1029/2005JD005810, 2005.

413 Lu, M. L. and Seinfeld, J. H.: Study of the aerosol indirect effect by large-eddy simulation of
414 marine stratocumulus. J Atmos Sci, 62, 3909-3932, doi:10.1175/jas3584.1, 2005.

415 Mather, G. K., Terblanche, D. E., Steffens, F. E., and Fletcher, L.: Results of the South
416 African cloud-seeding experiments using hygroscopic flares. J. Appl. Meteor., 36, 1433–
417 1447, 1997.

418 Rogers, R. R., and Yau, M. K.: A short course in cloud physics, Third Edition. International
419 Series in Natural Philosophy, Pergamon Press, Oxford, 290 pp, 1989.

420 Rosenfeld, D., Axisa, D., Woodley, W. L. and Lahav, R.: A quest for effective hygroscopic
421 cloud seeding, J. Appl. Meteorol. Climatol., 49(7), 1548–1562,
422 doi:10.1175/2010JAMC2307.1, 2010.

423 Rosenfeld, D., Lahav, R., Khain, A. and Pinsky, M.: The role of sea spray in cleansing air
424 pollution over ocean via cloud processes., Science, 297, 1667–1670,
425 doi:10.1126/science.1073869, 2002.

426 Russell, L. M., Sorooshian, A., Seinfeld, J. H., Albrecht, B. A., Nenes, A., Ahlm, L., Chen, Y.
427 C., Coggon, M., Craven, J. S., Flagan, R. C., Frossard, A. A., Jonsson, H., Jung, E., Lin, J.
428 J., Metcalf, A. R., Modini, R., Mülmenstädt, J., Roberts, G. C., Shingler, T., Song, S.,
429 Wang, Z. and Wonaschütz, A.: Eastern pacific emitted aerosol cloud experiment, Bull.
430 Am. Meteorol. Soc., 94, 709–729, doi:10.1175/BAMS-D-12-00015.1, 2013.

431 Segal, Y., Khain, A., Pinsky, M. and Rosenfeld, D.: Effects of hygroscopic seeding on
432 raindrop formation as seen from simulations using a 2000-bin spectral cloud parcel model,
433 Atmos. Res., 71, 3–34, doi:10.1016/j.atmosres.2004.03.003, 2004.

434 Segal, Y., Pinsky, M. and Khain, A.: The role of competition effect in the raindrop formation,
435 Atmos. Res., 83, 106–118, doi:10.1016/j.atmosres.2006.03.007, 2007.

436 Slingo, A.: Sensitivity of the Earth's radiation budget to changes in low clouds, Nature, 343,
437 49–51, doi:10.1038/343049a0, 1990.

438 Sorooshian, A., Wang, Z., Feingold, G. and L'Ecuyer, T. S.: A satellite perspective on cloud
439 water to rain water conversion rates and relationships with environmental conditions, J.
440 Geophys. Res. Atmos., 118(12), 6643–6650, doi:10.1002/jgrd.50523, 2013.

441 Takahashi, T.: Warm rain, giant nuclei and chemical balance-A numerical model, J. Atmos.
442 Sci., 33, 269-286, 1976.

443 Tzivion, S., Reisin, T. and Levin, Z.: Numerical simulation of hygroscopic seeding in a
444 convective cloud, J. Appl. Meteorol., 33, 252-266,1994.

445 Yin, Y., Levin, Z., Reisin, T. G. and Tzivion, S.: The effects of giant cloud condensation
446 nuclei on the development of precipitation in convective clouds — a numerical study,
447 Atmos. Res., 53(1-3), 91–116, doi:10.1016/S0169-8095(99)00046-0, 2000a.

448 Yin, Y., Levin, Z., Reisin, T. G. and Tzivion, S.: Seeding convective clouds with hygroscopic
449 flares: Numerical simulations using a cloud model with detailed microphysics, J. Appl.
450 Meteorol., 39, 1460–1472, 2000b.

451 World Meteorological Organization: Report of the WMO workshop on hygroscopic seeding.
452 WMP Rep. 35, WMO/TD 1006, Geneva, Switzerland, 68 pp, 2000.

453 Zhang, L., Michelangeli, D. V. and Taylor, P. a.: Influence of aerosol concentration on
454 precipitation formation in low-level, warm stratiform clouds, J. Aerosol Sci., 37(2), 203–
455 217, doi:10.1016/j.jaerosci.2005.04.002, 2006.

Zheng, X., Albrecht, B., Jonsson, H. H., Khelif, D., Feingold, G., Minnis, P., Ayers, K., Chuang, P., Donaher, S., Rossiter, D., Ghate, V., Ruiz-Plancarte, J. and Sun-Mack, S.: Observations of the boundary layer, cloud, and aerosol variability in the southeast Pacific near-coastal marine stratocumulus during VOCALS-REx, Atmos. Chem. Phys., 11(18), 9943–9959, doi:10.5194/acp-11-9943-2011, 2011.

Appendix A : Summary and Flight patterns of salt seeding experiments.

During E-PEACE, salt powder was ejected into cloud decks during nine flights. To better understand the individual seeding cases, the summary of salt seeding experiments is given in Table A1.

Table A1. Summary of salt seeding experiments

Date	Description	Cloud level (m) from Table 4 of Russell et al. (2015)
7/8	The TO did not sample the cloud after salt seeding. No post-seeding legs.	257-362 m (Thin cloud layer)
7/9	We performed two salt seeding experiments. However there was no post-seeding cloud-sampling leg for the first experiment. For the second experiment, the reference cloud legs (i.e., non-salted cloud sampling legs) were possibly contaminated by the first salt seeding experiment by the method shown in Fig. 5	283-570 m (Thick, wet cloud layer)
7/26	The seeding/sampling strategy was not an ideal (seeding and sampling pattern was perpendicular, and there was no sufficient post-seeding sampling). During the post-seeding flights in the mid-cloud and cloud-base heights, the seeded area was already advected far southeast. Only cloud top legs (post-seeding flight) were sampled from the estimated seeding area, and the seeding effects were shown at least in the cloud top leg.	253-560 m (Thick cloud layer)
7/29	NO post-seeding sampling legs. Right after injecting salt power, TO sampled the cloud at the same height as seeding, but it was found that the TO flew slightly	265-534 m (High wet clouds)

	above the seeding height (no LWC is detected).	
8/2	The seeding/sampling strategy was not an ideal. Intersection with seeded area was small since the post-seeding was not made in the downstream of the seeding area. Seeding effect was not seen.	310-613 m (Thick, wet cloud layer)
8/3	Descent case solely based on the strategy (shown in the manuscript)	309-628 m (Thick cloud), *H~369 m
8/10	Descent case solely based on the strategy. However the cloud was already precipitating when it was seeded.	286-553 m (low clouds) *H~367m
8/11	The seeding/sampling strategy was not an ideal. During the mid-and cloud-top legs (post-seeding flight), the seeded area was already advected far southeast. Only cloud-base legs were (barely) located within the seeded area.	440-600 m (Two broken cloud layers)
8/12	The seeding/sampling strategy was not an ideal. Post-seeding cloud sampling leg on the cloud-base only (barely) sampled the seeded area (no sufficient data for the post-seeding legs).	278-578 m (Thick cloud layer)

*H (cloud thickness) is calculated from the vertical profile of LWC obtained from soundings on the day.

According to Table A1, there were four less-than-ideal and two ideal cases of seeding experiments in terms of seeding and sampling strategy. Flight patterns of those six seeding experiments are shown in Fig. A1.

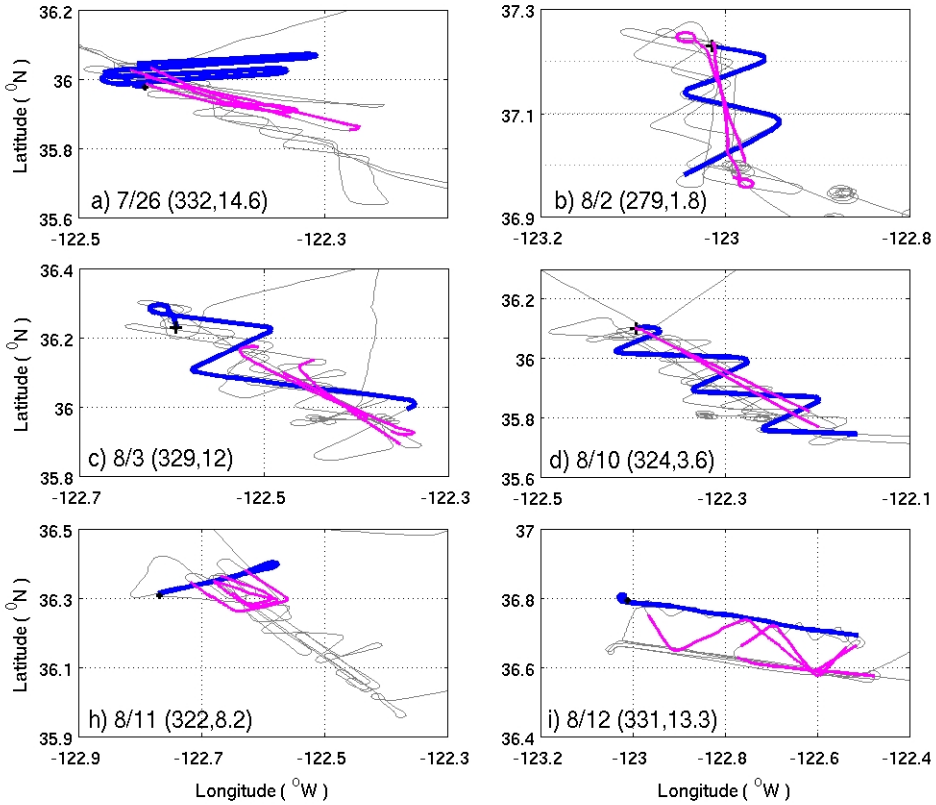

474

475 **Fig. A1.** Flight patterns during salt seeding (blue) and post-seeding cloud sampling legs
476 (magenta) for some of the seeding flights. First and second numbers inside the parenthesis
477 indicate the mean wind speed and wind direction during the salt-seeding leg, respectively.

478

479 Figure A1 showed that the parallel post-seeding sampling with zigzag seeding pattern (c and d; 3
480 August and 10 August 2011) was found to be the most effective flight pattern to capture the
481 seeding effects. In contrast, the perpendicular patterns between the seeding and post-seeding
482 patterns reduced the chance of proper sampling of a salted/seeded air mass during the post-
483 seeding flights. In this case, there was no sufficient time for the seeded air mass to be sampled
484 during the post-seeding sampling legs.

485

Table 1. GCCN concentrations obtained from CAS on 3 August 2011

	Near ocean surface (leg b in Fig. 4a)	~750 m (~ 17UTC)
Diameter (μm)	Concentrations (cm^{-3})	Concentrations (cm^{-3})
D > 2	1.89	5×10^{-2}
D > 10	5.4×10^{-2}	3×10^{-3}
D > 20	9.5×10^{-3}	-

488 **Table 2**. Summary of flight legs and soundings during the flight on 3 August 2011.

-	Pre-seeding legs			Seeding	Post-seeding legs			Clear-sky (boundary layer) legs				Soundings	
Flight level-leg	Cloud-base	Mid-cloud	Cloud-top (CT)	Seeding at CT	Cloud-base	Mid-cloud	Cloud-top	Sub-cloud layer			Above CT	ascents	descents
Shown in Fig. 4	c	d	e	f	g	h	I	b	f	f	j	black	red
Flight time (hh:mm:ss)	17:21:00-17:38:24	17:39:36-17:58:12	18:02:24-18:22:48	18:02:00-18:20:00	18:48:36-18:55:48	18:57:00-19:06:54	19:09:54-19:17:24	17:06:54-17:18:36	18:27:36-18:34:30	18:36:00-18:46:69	19:18:00-19:22:48	16:52:15-16:58:19	17:06:47-17:10:48
Flight heights	339 m	481 m	582 m	582 m	307 m	421 m	594 m	24 m	22 m	175 m	669 m	-	-
Flight direction	NW to SE	SE to NW	NW to SE	NW to SE	NW to SE	SE to NW	NW to SE	SE to NW	SE to NW	SE to NW	SE to NW	-	-

489

490

491 **Table 3**. The mean value of effective diameter D, number concentrations N_d of cloud droplets, precipitation rate, R , and the median
492 value of calculated radar reflectivity Z on 3 August 2011 for pre- and post-seeding legs at cloud top, mid-cloud and cloud-base heights.
493 D shown in the parenthesis is calculated from drop size distributions obtained by combining the CAS and CIP probes.

8/3/2011	D (μm)		N_d (cm^{-3})		R ($mm\ hr^{-1}$)		LWC ($g\ m^{-3}$)		Z (dBz)	
Legs	Pre-seeding	Post-seeding	Pre-seeding	Post-seeding	Pre-seeding	Post-seeding	Pre-seeding	Post-seeding	Pre-seeding	Post-seeding
Top	21.4 ± 4.9 (22.9 ±7.1)	26.2 ± 3.4 (29.9 ± 8.8)	143 ± 77	70 ± 24	0.09 ± 0.27	0.21 ± 0.57	0.31±0.10	0.25±0.06	-31.8	-17.1
Mid	17.2 ± 2.39 (18.1± 4.7)	18.1 ± 2.8 (23.9 ± 9.3)	171 ± 46	100 ± 42	0.06 ± 0.28	0.17 ± 0.49	0.26±0.05	0.12±0.05	-32.1	-16.3
Base	13.5 ± 1.7 (15.0 ± 3.8)	16.6 ± 7.0 (44.3 ± 37.4)	162 ± 56	77 ± 50	0.04 ± 0.14	0.16 ± 0.50	0.09±0.09	0.04±0.03	-31.0	-13.8

Table 4. Total droplets number concentrations larger than critical sizes. Numbers are average concentrations at three cloud levels.

	Before (cm^{-3})	After (cm^{-3})	Difference (cm^{-3})
D > 50 μm	0.4	0.6	0.2
D > 100 μm	1.6×10^{-2}	4.7×10^{-2}	3.2×10^{-2}
D > 200 μm	3.1×10^{-4}	1.2×10^{-3}	3.4×10^{-4}

498 **Figure captions**

499

500 **Fig. 1.** Relative (percent of total) a) number and b) volume distributions of powdered salt
501 delivered to CAS sampling volume from atomizer.

502

503 **Fig. 2.** A pictorial schematic and photo of the salt powder delivery system.

504

505 **Fig. 3.** Profiles of (a) potential temperature (θ, K), (b) liquid water contents (LWC, g kg^{-1}), and
506 (c) accumulation mode aerosol concentrations (#/cc, PCASP) during the aircraft ascent (black)
507 and descent (red) between 16:52:15-17:10:48 UTC (hh:mm:ss). Aerosol concentrations obtained
508 from sub-cloud layer and above cloud layer are shown as grey colors (mean value is shown as
509 cyan square). The heights and spatial locations of data used are shown in Fig. 4. PCASP resolves
510 particles in diameter ranges from 0.1-3 μm.

511

512 **Fig. 4.** (a) Time series of flight altitudes and (b-j) flight paths on 3 August 2011. The flight
513 pattern for salt seeding is shown as thick blue colors in Fig. 4(f-j). The mean wind speed (12 m s^{-1})
514 and direction (329 °) for the seeding period are shown in Fig. 4f. Individual legs with
515 corresponding colors are shown in each box accordingly. The detailed information of each level
516 leg, such as flight heights and duration, is summarized in Table 2.

517

518 **Fig. 5.** Salt seeding pattern (blue) with estimated advected seeding area at (a) cloud top, (b) mid-
519 cloud and (c) cloud base. The seeding and post-seeding cloud sampling areas are shown as blue
520 and red colors, respectively, at each level. The estimated seeding area for the post-seeding flights
521 are shown as gray shades. The darker gray area points are the advected points calculated with the
522 shorter possible elapsed times.

523

524 **Fig. 6.** Changes in cloud droplets' (a) size, (b) number concentration, and (c) drizzle rate during
525 cloud-base, mid-cloud and cloud top legs on 3 August 2011. Data obtained from pre-seeding legs
526 (1-second values) are shown as grey (mean value as yellow square); data obtained from post-
527 seeding flights are shown as red (mean value as blue square). (b) and (c) are calculated from drop
528 size distribution (DSD) obtained from CAS and CIP probes, respectively. (a) is calculated from
529 DSDs obtained by combing the CAS and CIP probes.

530

531 **Fig. 7.** Drop size distributions (DSDs) obtained from level legs at (a) cloud top, (b) mid-cloud,
532 and (c) cloud base before (blue) and after (red) seeding on 3 Auguest 2011. DSDs are calculated
533 from CAS (thin) and CIP (thick) probes for the pre- and post-seeding legs. "BEFORE" and
534 "AFTER" indicates pre- and post-seeding legs, respectively. The values are based on the
535 averages for each level leg, shown in Fig. 4 and Table 2.

536

537 **Fig. 8.** (a) The radar reflectivity (in dBz, reflectivity Z is proportional to D^6 of droplet diameters)
538 shows precipitation above the cloud radar in (a) an area of cloud sampled before seeding and the

539 (b) same air mass sampled after seeding during cloud-base level leg. Y axes in (a)-(c) indicates
540 the altitudes above the radar during the cloud-base level leg. The drizzle rates in (a) and (b) are
541 estimated from the CIP (units of hundredth of mm day^{-1}). The outlined box in panel (b) indicates
542 where a detailed analysis is made for (c) the radar reflectivity in dBz and d) drizzle rates (from
543 CIP) in mm day^{-1} and the cloud liquid water content (from PVM-100) in g m^{-3}.

544

545 **Fig. 9.** As in Fig. 6, but for 10 August 2011, where the cloud is initially precipitating at the time
546 of seeding. Data obtained from pre-seeding legs are shown as grey (mean value as black square);
547 data obtained from post-seeding legs are shown as red (mean value as blue square). Median
548 value of drizzle rates are shown as cross symbols in Fig. 9(c).

549

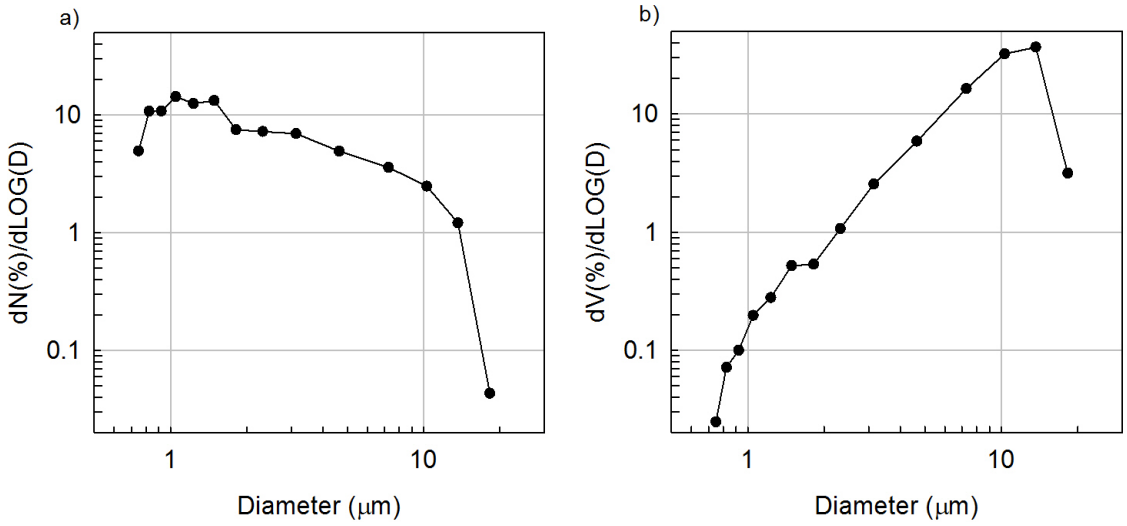

550

551 **Fig. 1.** Relative (percent of total) a) number and b) volume distributions of powdered salt

552 delivered to CAS sampling volume from atomizer.

553

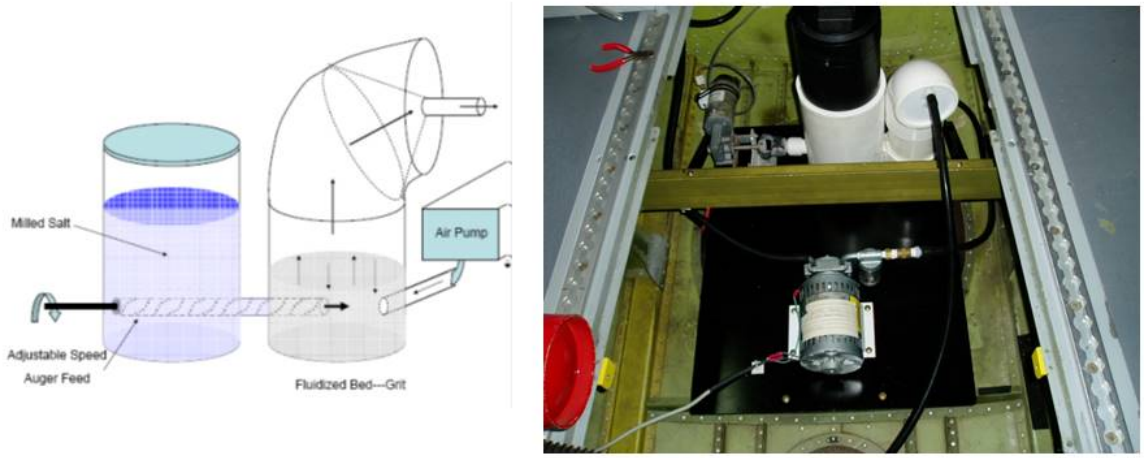

554

555 **Fig. 2.** A pictorial schematic and photo of the salt powder delivery system.

556

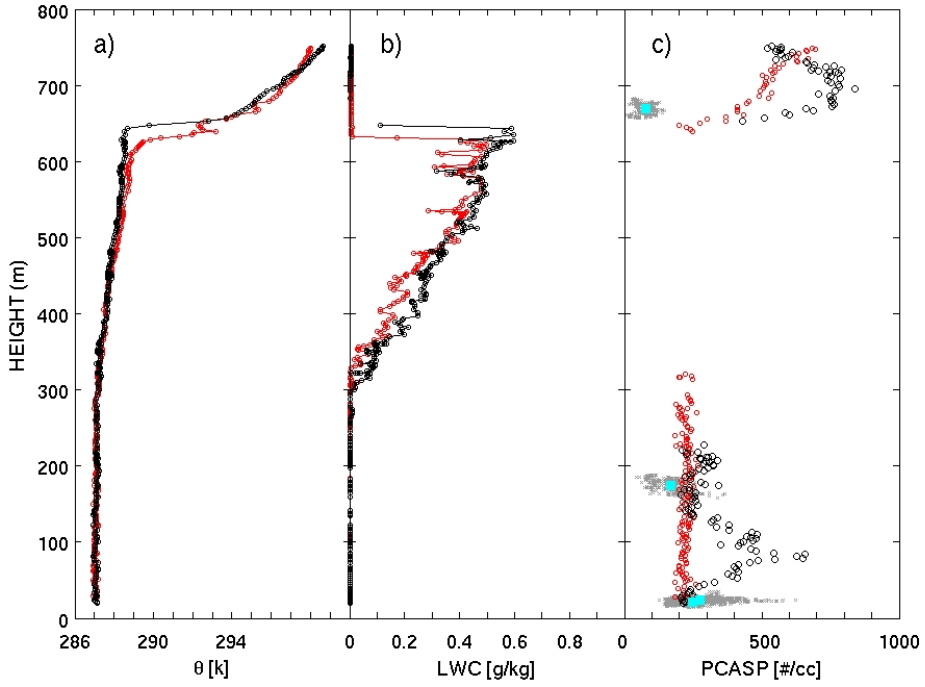

557

558 **Fig. 3.** Profiles of (a) potential temperature (θ , K), (b) liquid water contents (LWC, g kg^{-1}), and

559 (c) accumulation mode aerosol concentrations (#/cc, PCASP) during the aircraft ascent (black)

560 and descent (red) between 16:52:15-17:10:48 UTC (hh:mm:ss). Aerosol concentrations obtained

561 from sub-cloud layer and above cloud layer are shown as grey colors (mean value is shown as

562 cyan square). The heights and spatial locations of data used are shown in Fig. 4. PCASP resolves

563 particles in diameter ranges from 0.1-3 μm.

564

565

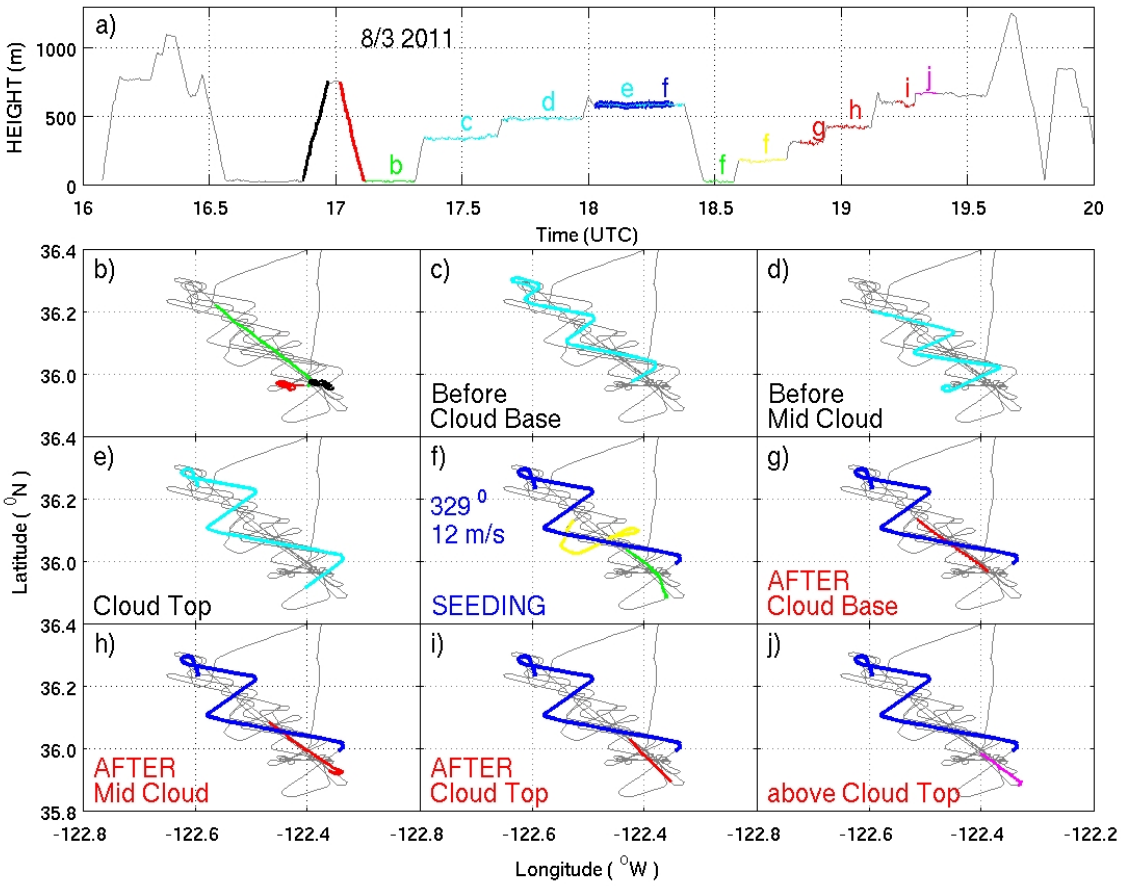

566

567 **Fig. 4.** (a) Time series of flight altitudes and (b-j) flight paths on 3 August 2011. The flight
568 pattern for salt seeding is shown as thick blue colors in Fig. 4(f-j). The mean wind speed (12 m s^{-1})
569 and direction (329 °) for the seeding period are shown in Fig. 4f. Individual legs with
570 corresponding colors are shown in each box accordingly. The detailed information of each level
571 leg, such as flight heights and duration, is summarized in Table 2.

572

573

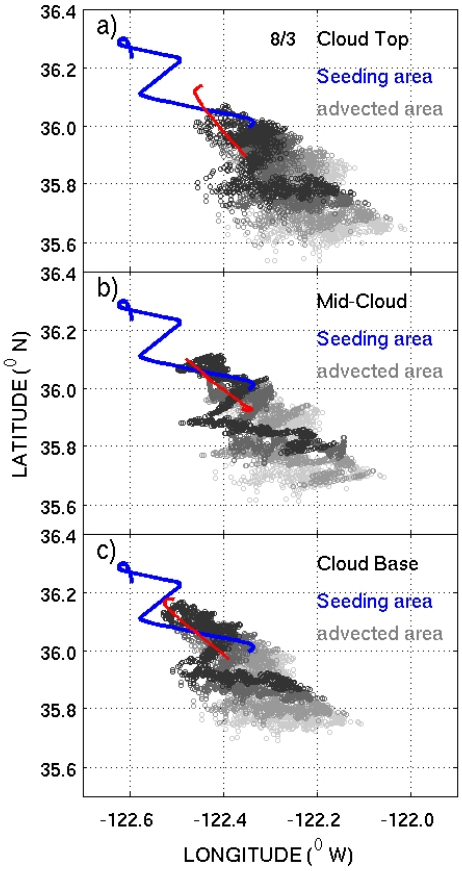

574

575 **Fig. 5.** Salt seeding pattern (blue) with estimated advected seeding area at (a) cloud top, (b) mid-
576 cloud and (c) cloud base. The seeding and post-seeding cloud sampling areas are shown as blue
577 and red colors, respectively, at each level. The estimated seeding area for the post-seeding flights
578 are shown as gray shades. The darker gray area points are the advected points calculated with the
579 shorter possible elapsed times.

580

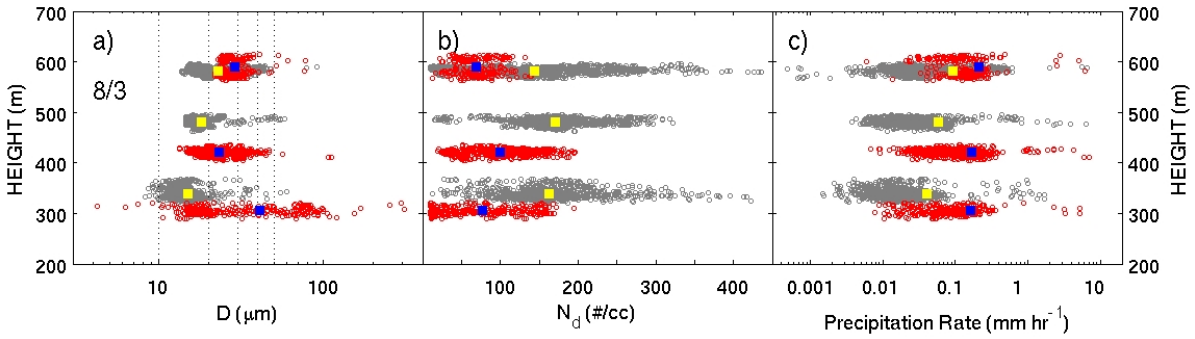

581

582 **Fig. 6.** Changes in cloud droplets' (a) size, (b) number concentration, and (c) drizzle rate during
583 cloud-base, mid-cloud and cloud top legs on 3 August 2011. Data obtained from pre-seeding legs
584 (1-second values) are shown as grey (mean value as yellow square); data obtained from post-
585 seeding flights are shown as red (mean value as blue square). (b) and (c) are calculated from drop
586 size distribution (DSD) obtained from CAS and CIP probes, respectively. (a) is calculated from
587 DSDs obtained by combing the CAS and CIP probes.

588

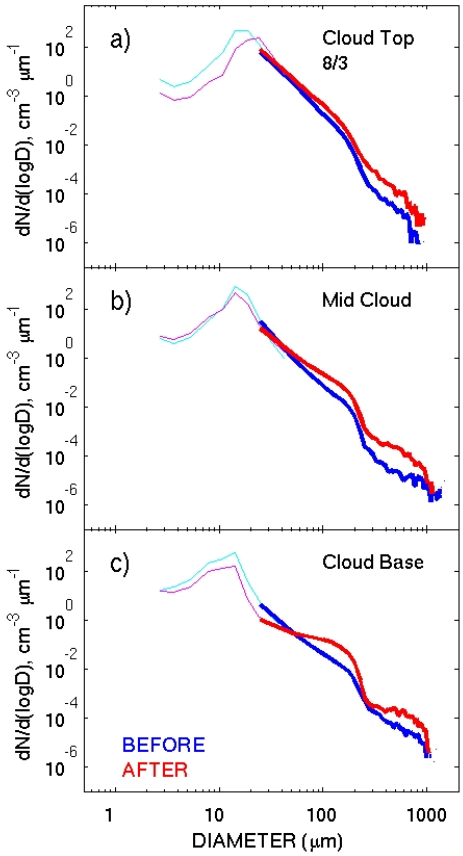

589

590 **Fig. 7.** Drop size distributions (DSDs) obtained from level legs at (a) cloud top, (b) mid-cloud,
591 and (c) cloud base before (blue) and after (red) seeding on 3 Auguest 2011. DSDs are calculated
592 from CAS (thin) and CIP (thick) probes for the pre- and post-seeding legs. "BEFORE" and
593 "AFTER" indicates pre- and post-seeding legs, respectively. The values are based on the
594 averages for each level leg, shown in Fig. 4 and Table 2.

595

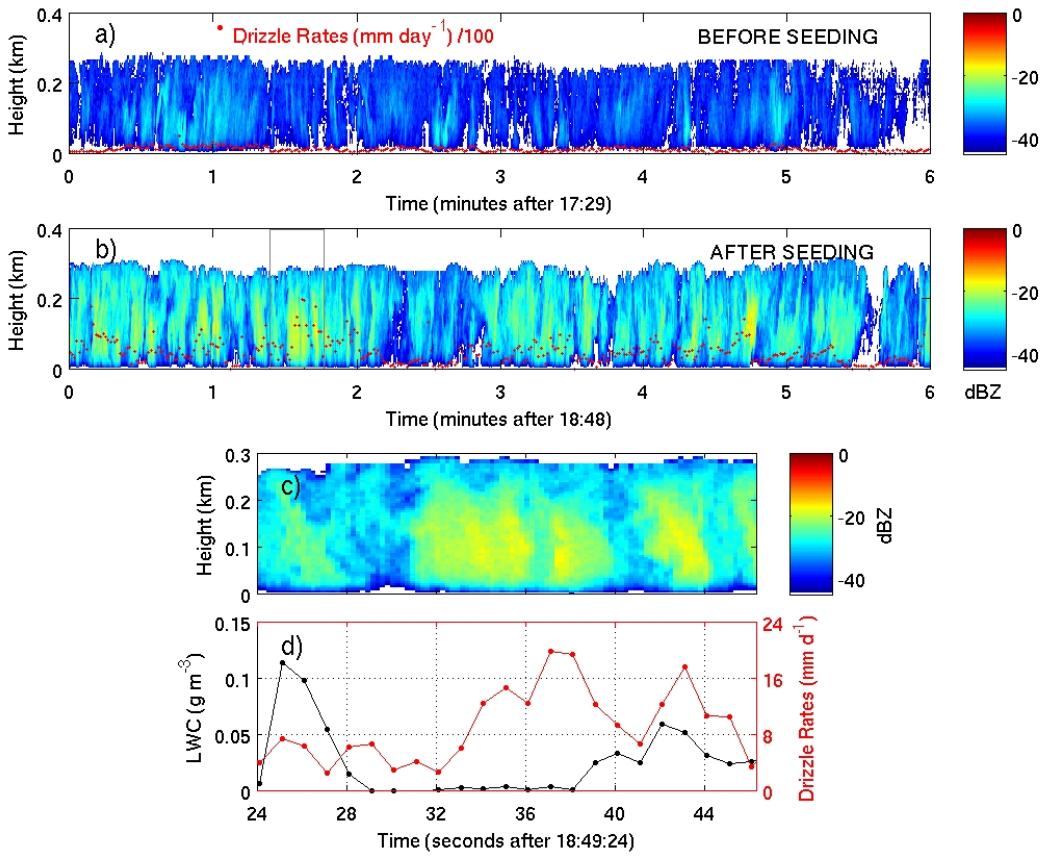

596

597 **Fig. 8.** (a) The radar reflectivity (in dBz, reflectivity Z is proportional to D^6 of droplet diameters)
598 shows precipitation above the cloud radar in (a) an area of cloud sampled before seeding and the
599 (b) same air mass sampled after seeding during cloud-base level leg. Y axes in (a)-(c) indicates
600 the altitudes above the radar during the cloud-base level leg. The drizzle rates in (a) and (b) are
601 estimated from the CIP (units of hundredth of mm day^{-1}). The outlined box in panel (b) indicates
602 where a detailed analysis is made for (c) the radar reflectivity in dBz and d) drizzle rates (from
603 CIP) in mm day^{-1} and the cloud liquid water content (from PVM-100) in g m^{-3}.

604

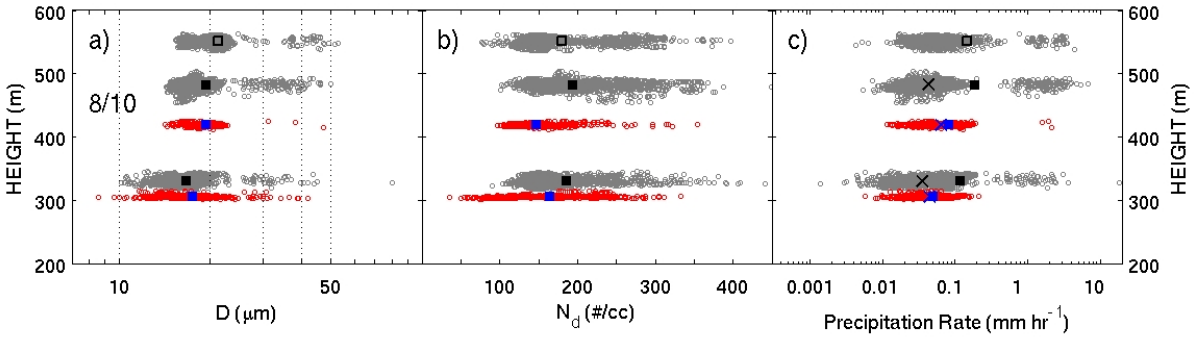

605

606 **Fig. 9.** As in Fig. 6, but for 10 August 2011, where the cloud is initially precipitating at the time
607 of seeding. Data obtained from pre-seeding legs are shown as grey (mean value as black square);
608 data obtained from post-seeding legs are shown as red (mean value as blue square). Median
609 value of drizzle rates are shown as cross symbols in Fig. 9(c).

610